Microfluidic approaches for accessing thermophysical properties of fluid systems

Théo Gavoille, Nicolas Pannacci, Ghislain Bergeot, Claire Marlière, Samuel Marre

Microfluidic approaches for accessing thermophysical properties of fluid systems

Theo Gavoille[a,b], Nicolas Pannacci[a], Ghislain Bergeot[a], Claire Marliere[a], Samuel Marre[b]

Thermophysical properties of fluid systems are highly desirable as they are used in many industrial processes both from a chemical engineering point of view and also to push forward the development of modeling approaches. To access these data, microfluidic approaches have recently attracted increasing interest as they provide flexible and reliable ways for measurements, leading to fast screening capabilities compared to the conventional experimental systems. In this review, we present a general overview of microfluidic methodologies integrating *in situ* characterization to determine thermodynamic properties of fluid systems. In addition to drastically reducing the time to reach thermodynamic equilibria, one major advantage of microfluidics is to provide an optical access to the fluid behavior, even in harsh conditions. Therefore, several *in situ* characterization techniques can be implemented to get insights in fluids properties. In here, we emphasize approaches developed using high pressure and high temperature microfluidics. Indeed, such conditions are of interest for energy industries and present plenty of challenges. Several recent examples of high pressure microfluidics optical approaches will be detailed, in particular to determine viscosity and density, phase equilibria, mass transfer coefficient and solubility parameters.

Introduction

The determination of fluid thermodynamic properties is critical to a wide range of industrial applications such as gas treatment, biomass energy process or Enhanced Oil Recovery (EOR). Although thermodynamic models have been developed, they are not always adapted. Indeed, according to the operating conditions and the type of fluids, a specific equation of state (Virial equation of state, Peng Robinson equation of state…) or activity coefficient models have to be chosen. Therefore, the need for experimental data is still very crucial. Being able to perform fast and accurate properties measurements with low quantities of product is a major challenge Industries are working on for financial and schedule reasons. In addition, when high pressure and high temperature conditions are required for the measurements, traditional methods are time- and money- consuming. In fact, if the thermodynamic properties characterization technique requires a homogenous fluid mixture, industries and research laboratories traditionally use Pressure-Volume-Temperature (PVT) cells[1] to reach the thermodynamic equilibrium under the right conditions. This kind of equipment requires volumes of fluids ranging from *50 ml* to a few liters which are introduced in a pressurized column, equipped with a transparent window for getting an optical access. The fluid pressure is applied by a piston and the entire PVT cell is placed in a heated chamber for controlling the temperature. The mass of fluid in the PVT cell, along with the construction material of the cell, imply a major thermal inertia. Consequently, reaching the phase equilibrium in such systems usually takes several hours[2,3]. Moreover, the amount of energy to reach and maintain the temperature can be high. In terms of safety, a small fabrication defect in such systems could easily causes an explosion that might results in severe injuries to the operators or damages in equipment.

To address these problems, microfluidics is an appropriate support. Thanks to the small mass to heat and channel dimensions (tenths to hundreds of micrometers in width and depth), thermodynamic equilibrium can be reached in minutes, even miliseconds[4]. Concurrently, since energy, product consumption and safety are all critical parameters to consider, microfluidics provides an efficient alternative to conventional experimental tools. By means of the small volumes (few microliters) in the micro-reactors, microfluidics allows working in energy efficient and safe environments. Eventually, the recent development of microfabrication techniques have provided microdevices with enhanced mechanical and thermal properties for working under high pressure and high temperature conditions[5] which can be adapted to meet the conditions required for most of characterization methods.

In this context, the purpose of this review is to give a broad overview of the existing microfluidic optical approaches for *in situ* fluids thermodynamic properties characterization with a focus on high pressure and high temperature, as such conditions are of interest for chemical engineering and energy applications among others. In particular, we have targeted the determination of the viscosity and density, phase equilibria, mass transfer coefficients and the solubility determination. Microfluidic devices developed to access these demanding conditions will be first introduced to understand issues that may occur in the compatibility with characterization instrumentations. The adaptation of characterization techniques to microfluidics for *in situ* fluids thermodynamic properties determination and the associated constraints will be outlined as well as some methodologies developed for case studies. Subsequently, for each property, an overview of *in situ* microfluidic strategies will be presented through examples along with upgrades made on equipment and methodologies.

High pressure and high temperature microfluidics

In the early years of microfluidics, the scope of applications was limited by the materials that were employed. With the development of nanotechnologies came new micro-manufacturing techniques and microdevices have been perfected, allowing the use of a wider range of materials. New microfluidic devices are now allowing to work under high pressure and high temperature conditions with a wide variety of fluids. Along with these new devices and materials, new challenges for thermodynamic properties characterization have arisen. In this section, we will review technologies used for high pressure and high temperature microfluidic devices fabrication along with *in situ* characterization methods that have been developed to investigate fluids flows under such demanding conditions.

Microfabrication techniques for accessing high pressures and temperatures on a chip

The first microsystems allowing to work under high pressure and high temperature condition were simple tubing made with stainless steel or silica[6]. These systems are still used to study jets breakup regimes for example[7], however, they are rather limited in term of design. Since, more complex devices have been developed, in particular on a chip, resulting in a wide range of designs in two to three dimensions. This design flexibility provided by microfabrication allows for precise manipulation of hydrodynamics and fast mixing, which are typically needed for the study of fluid flows and thermodynamics. In particular, Marre *et al.*[8] have extensively reviewed the fabrication approaches and developments in microfluidics processes under supercritical conditions. Several materials can be chosen depending on the targeted applications and conditions that are required.

i. Microfabrication materials

Metal microfluidic devices can be manufactured by electroforming, electro-discharge machining or laser ablation[1]. They can hold several hundreds bar of pressure and high temperature conditions (up to *800 °C* when considering nickel based alloys). They are also chemically compatible with a wide range of fluids except for strong acids. However, the main limitation is the absence of optical accesses inside the channels.

Similarly, ceramic micro-reactors do not provide optical access but are well adapted to high temperature processes and applications as they can withstand high temperatures (up to *1200 °C*) and exhibit good chemical resistances. Their pressure compatibility is however rather poor and manufacturing costs can be expensive. Modular ceramic micro-reactors have been developed[9] using standard molding techniques. These devices do not necessarily required to be manufactured in a clean room environment. However, current machining tools are not precise enough and the precision on the channel dimensions would be in the order of tens of microns.

To benefit from the advantage of *in situ* monitoring of fluids flow, it is necessary to provide an optical access into microfluidic channels by considering transparent microfabrication materials. For instance, glass-glass microdevices are etched with Hydrofluoric acid (HF) or BOE (Buffer Oxide Etchant)[10] and are thermally bonded. These micro-reactors offer an easy optical access for in situ characterization techniques. Depending on the channel dimensions, such devices are compatible with pressures up to *400 bar*[11] under reasonable temperature conditions. However, given the poor thermal conductivity value of the glass, such devices do not allow quick and homogenous temperature changes, which can lead to a temperature gradient across the chip. The optical access, the low cost manufacturing technique and the commercial availability make these devices widely used for research applications at room temperature and pressure up to *50 bar* with commercial devices and up to *400 bar* with lab built devices.

Additionally, silicon-borosilicate microdevices have the advantage to allow performing experimentations under even higher pressure and temperature conditions (up to *400 °C* and *300 bar*[5]). They are made through silicon etching with further anodic bonding to a borosilicate wafer. The high thermal conductivity value of the silicon allows a good control of the device's temperature. High pressure can be reached and the borosilicate side still provides an easy optical access[5]. These devices provide a mean for the implementation of a wide range of *in situ* characterization methods.

In brief, for a considered study, the choice of the microfluidic device will depend on the type of fluids flowing through the system regarding the device dimensions (and the associated pressure drop) but also its chemical compatibility. Concerning the thermomechanical stability, the maximum pressure the microsystem can withstand will depend on the construction materials, the temperature[5], the surface area out of which the pressure is applied (*i.e.* the channels dimensions and geometry)[5,11] and the bonding quality. The parameters to considered were already reported in a former study[5].

The ability to have an excellent control of the operating conditions is essential in the acquisition of experimental thermodynamic data. The main parameters to control are the temperature, the pressure and the flow rates (when working on fluid mixtures).

ii. The importance of temperature control on chip

Due to the size of microfluidic devices, the temperature is a challenging parameter to control and measure, when some areas of the chip need to remain available for in situ characterization. Several heating and cooling modules for microfluidic devices have been developed and reviewed over the last decades[12], but most of them are applied to low pressure microfluidics. When working with devices capable of performing under high pressure conditions, materials and manufacturing protocols are so strict that integrating heating components to the chips is a challenge. All of the methods applied to high pressure microfluidics encountered in the literature involve an external heating or cooling module. Local homogenous temperatures on a microfluidic device have been applied by immersing the device in a temperature controlled bath[7], by contacting the device to electrical heater[13,14] or to Peltier elements[15,11] (Figure 1 (a) and (b)). A more sophisticated device has been developed by Lao et al.[16], indeed, using sputtering processes, they deposited nanolayers of platinum and titanium layers as heater and temperature sensors. Microwaves[17] have also been used to heat locally a glass-glass microfluidic device (Figure 1 (c)).

Temperature gradients can also be applied over microfluidic devices by combining thermostated fluids flowing in metallic blocks contacting different zones of the device and heating cartridges[18,19].

The temperature of a microfluidic device can be measured using external or internal probes. The former case is simpler to implement and temperature sensors such as resistors or thermocouples can be put in contact with the external surface of the microdevice[13]. However, the precision of such approaches is highly dependent upon (i) the mode in which the microreactor is used (flow or batch) and (ii) the thermal conductivity of the construction materials. Silicon-based microreactors, therefore, exhibit improved temperature measurements than glass-based microdevices thanks to the higher thermal conductivity of silicon ($149\ W.m^{-1}.K^{-1}$), compared to most of the glasses ($\approx 1\ W.m^{-1}.K^{-1}$).

Temperature measurements using internal probes require more complicated fabrication processes, yet the probe is in direct contact with the fluid, leading to higher confidence in the measurement. Such devices integrating in situ temperature sensors have been widely developed for polymer based microfluidics (documented in a review written by Miralles *et al.*[12]). Recently, these tools have been extended to high pressure microfluidics, Andersson *et al.*[20,21] managed to integrate thin film metal heater and temperature sensors in fusion bonded glass chips in order for the system to act as a flow sensor.

Other means to measure temperature inside a microreactor include thermal cameras[15], which can also be employed, taking into account reflection or transparency issues or the use of a reference fluid[22] flowing in side microchannels placed next to the microchannel of interest, to have an indirect measurement / control of the temperature.

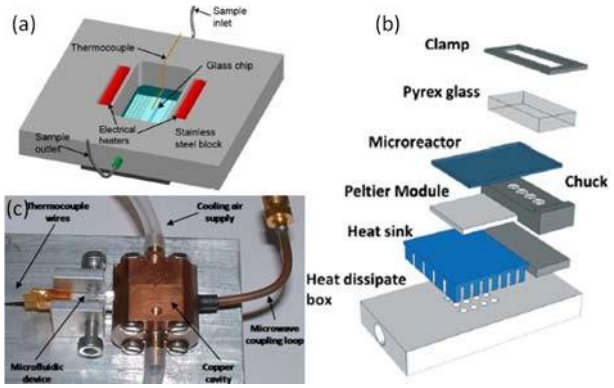

Figure 1: (a) Schematic of a microfluidic approach with high pressure, high temperature stainless steel chip holder. Heat cartridges maintained the temperature of the unit (Reproduced from ref. [14]. Copyright © 2014, American Chemical Society). (b) Schematic of a thermoelectric cooling system assembly (Reproduced from ref. [15]. © The Royal Society of Chemistry 2017) (c) Photograph of an experimental setup with a microwave heating device (Reproduced from ref. [17]. Copyright 2010 RSC publications).

In situ optical characterization approaches

Being able to access space and time-resolved information of thermodynamic properties of fluids in a non-intrusive way still presents challenges, which can be overcome by microfluidic approaches. Many existing macroscopic characterization methods can be adapted to work on microdevices. In this section, we will present some *in situ* characterization methods developed for microfluidics and which are also compatible in high pressure and high temperature environments provided that the systems are transparent to the wave length employed. We purposefully focused this review on optical characterization approaches but other characterization devices and methodologies are being developed, such as MEMS[23,24] which will only be mentioned.

i. Optical microscopy and high-speed cameras

One of the main interests of microfluidics is to have an optical access to the fluid inside the channels by simply using optical microscopy. These observations can be used to study the flow hydrodynamics, the formation, the disappearance or the evolution of interfaces, which can indicate a phase transition. Such phenomena can be extremely rapid at the microscopic scale, therefore, it is often necessary to monitor them by connecting a high-speed camera to an optical microscope. The combination with an image processing software can in some cases allow determining concentrations[25], diffusion coefficients[26], interfacial tensions[27,28], viscosities[29] etc. For instance, Zhu *et al*.[30] monitored the mass transfer of CO_2 chemical absorption into monoethanol amine (MEA) aqueous solutions under a Taylor flow in a T-junction micro-channel by measuring the volume of CO_2 bubbles along the channel with a high speed camera (Figure 2). The volume reduction observed of the CO_2 bubbles is directly linked to the CO_2 quantity dissolved into the solution.

Optical microscopy has also been exploited to monitor gas hydrates crystallization and dissociation[31]. Gas hydrates have a solid water-crystalline structure stabilized by a host molecule such as methane or carbon dioxide. Such clathrate compounds are a cause of numerous pipeline blockages in cold areas or in offshore production plants. More recently, natural methane clathrates found in cold regions (North Canada) or in seafloor sediments (for instance: Nankaï throat) are also investigated as a potential energy (gas) source. Hence, acquiring thermodynamic data about hydrates equilibrium stability is of high importance for energy industries. Jung *et al*.[32] investigated the kinetics of hydrates crystallization using image analysis on three different sets of experiments (in a capillary tube, between two surfaces and between spherical particles). In these experiments, CO_2 and CH_4

hydrates formation near the substrate was monitored using time-lapse pictures (Figure 3). Experiments were performed at *34 bar* for CO_2 hydrates, *80 bar* for CH_4 hydrates and *275 K* for both of them.

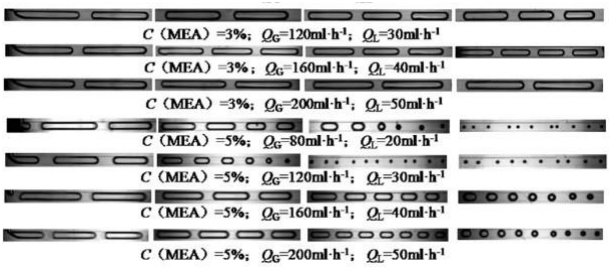

Figure 2: Pictures of a gas–liquid segmented flow CO_2 – MEA in a micro-reactor. CO_2 dissolves in monoethanol amine, leading to a slow decrease of CO_2 bubbles size, which can be monitored using optical microscopy (Reproduced from ref. [30]. Crown copyright 2014 Published by Elsevier Ltd. All rights reserved).

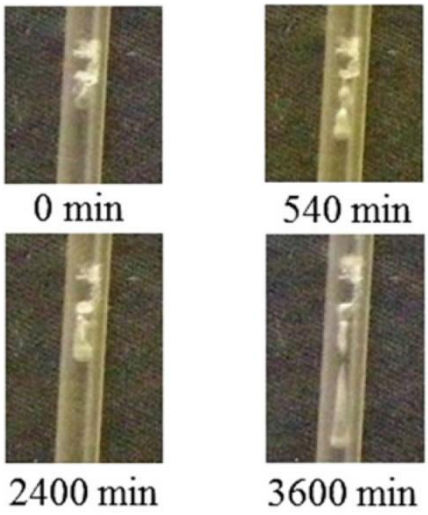

Figure 3: Time-lapse pictures of CO_2 hydrate formation and growth in a capillary tube (*275 K*, *34 bar*). The hydrate crystal starts crystalizing at the CO_2- water interface and propagates (Reproduced from ref. [32]. Copyright 2012 Elsevier B.V. All rights reserved).

ii. Fluorescence

Fluorescence is widely used in microfluidics as a detection tool for micro-sensing systems[33] but it can also be used to visualize and measure thermodynamic properties such as diffusion rate, solubility, miscibility and concentration fields. Fluorescence is a technique based on particles or molecules excitation. When excited at a specific wavelength, fluorophores emit back instantaneously at a different wavelength, which can be monitored independently from the excitation wavelength thanks to the use of specific filters. In 2001, Culbertson *et al.*[34] used fluorescence to compare four different microfluidic characterization methods used to measure diffusion coefficients. More details of their work and other diffusion measurements[35,36,37] are explained in the section *Mass transfer and solubility measurement strategies at microscale*. Fluorescence can also be used to determine the concentration of species since the signal intensity depends on the fluorophore concentration[25,38]. For instance, Nguyen *et al.*[39] lay on this principle to measure the minimum miscibility pressure of CO_2 in crude oils (Figure 4 (a)) using silicon-Pyrex® micro-reactors at a pressure of *60 bar*. Another approach has been developed by Kuhn *et al.*[40], they used a pH-sensitive laser-induced fluorescence technique (LIF) to monitor the mass transfer in a Taylor flow of CO_2 in alkaline solutions (Figure 4 (b)). The measured property is the pH of the alkaline solution and because dissolved CO_2 decreases the pH, the mass transfer can be monitored. This study was carried out in silicon-Pyrex® microdevices and they managed to highlight a connection between local mass transfer and secondary flow structures. Temperature variations inside a microfluidic channel can also be quantified by measuring the fluorescence intensity. Quinto-Su *et al.*[41] worked on that approach to monitor the temperature variations following single laser-induced cavitation inside a microfluidic gap.

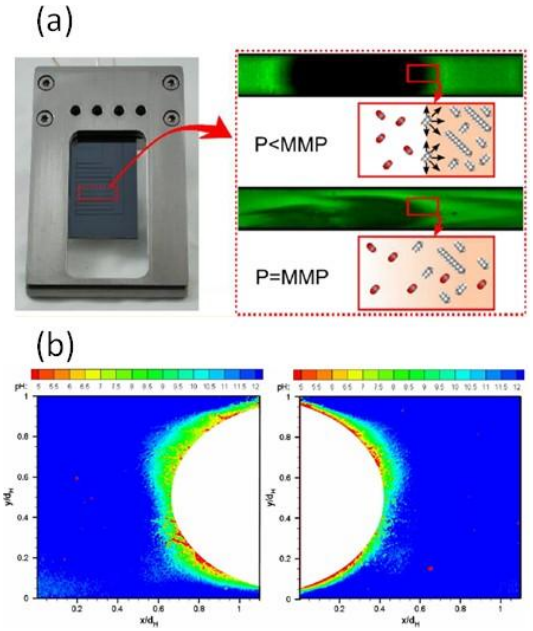

Figure 4: (a) Example of a Fast Fluorescence-Based microfluidic method to measure the minimum miscibility pressure of CO_2 in crude oils (Reproduced from ref. [39]. Copyright 2015, American Chemical Society). (b) Contours of the pH distribution at the back (left) and front (right) of a CO_2 bubble. This image was taken with a pH-sensitive laser-induced fluorescence approach (Reproduced from ref. [40]. Copyright 2012, American Chemical Society).

iii. µ-PIV

Being able to map the velocity field of a flow in a microfluidic channel can be of interest to classically quantify the residence time of fluids in complex structures (*e.g.* in case of a reaction) but also to understand mixing processes (appearance of dead zones with zero velocity or flow recirculation). Micro Particle Image Velocimetry (µ-PIV) is an *in situ* characterization approach that can provide better understanding of mixing phenomena at the microscale. Indeed, the mixing process in a microfluidic channel is mostly governed by diffusion, but microfluidic active or passive mixers have been developed[42,43] to accelerate this process. The operating principle of µ-PIV (similar to the one of PIV[44]) relies on the tracking of dispersed illuminated fluorescent particles in a fluid. The hypothesis made here is that these particles follow exactly the flow dynamics (*i.e.* (i) particles are small enough to avoid settling, they are monodispersed and (ii) they do not interact with walls). The velocity information is calculated by taking pictures at precise time intervals. The distance between each individual particle is measured between two images and the velocity field is obtained by dividing the displacement field by the time interval between the pictures.

Kinoshita *et al.*[45] developed a confocal µ-PIV equipment combining a high-speed confocal scanner with a conventional µ-PIV technique. The device enables to obtain cross-sectional particle images of droplets travelling in a micro-channel. The processed images show the 2D velocity distribution inside droplets at different focus positions (Figure 5). Therefore, 3D images can be computed on a small thickness (less than *50 µm* in that case).

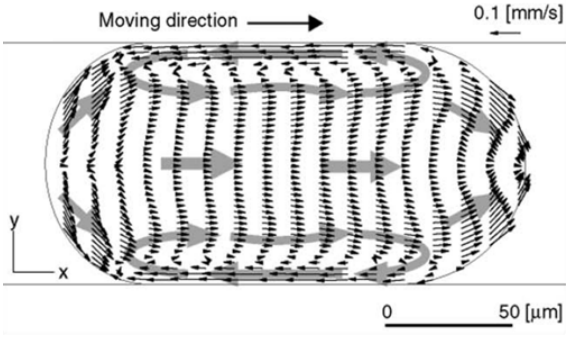

Figure 5: 2D velocity distribution of the cross-section of a droplet moving from left to right in a microfluidic channel. The arrow on the top right scales for *0.1 mm/s* and it represents the reference vector

(Reproduced from ref. [45]. Copyright 2007 RSC publications).

iv. UV-vis spectroscopy

Monitoring the evolution of molecule concentrations such as surfactant can be of interest for energy applications. Ultraviolet-visible (UV-vis) spectroscopy is a simple method to quantify a known molecule in a solution. This approach is based on molecule absorption. A solution is excited with a specific wavelength (between *100* and *800 nm*) of initial intensity I_0. Certain molecules can absorb this energy and therefore, the signal intensity is going to be smaller once it went through the solution containing this type of molecules. UV-vis is not the most effective method to identify an unknown molecule, however, it is an efficient approach to quantify the concentration of a known molecule as the Beer-Lambert law states that the absorbance A of the incoming light is proportional to the number of absorbing molecules.

In 2002, Petersen *et al*.[46] developed a silicon-borosilicate microdevice integrated waveguides and a long path length detection cell for UV-vis spectrometry. In their work, they compared electrophoretic separation performances and sensitivity of molecules such as caffeine, paracetamol or ascorbic acid using their absorbance with different approaches (using conventional capillary electrophoresis instruments and an on-chip U-cell). They found their microchip with the integrated U-cell and in plane waveguides to have a sensitivity between *9* and *22* times higher than in capillaries (with inner diameter of *50* and *75 µm*) in a conventional electrophoresis. Later on, Yue *et al*.[47] reported the use of a more sophisticated commercial device, a glass microfluidic chip with integrated waveguides for UV-vis absorbance detection in the evanescent wave field. They only demonstrated its capabilities performing UV-vis detection of a segmented flow of N_2 bubbles into water. To do so, they monitored the synthesis of gold nanoparticles (GNP) in droplets flowing in a segmented flow in a PTFE capillary micro-reactor using UV-is spectrometry (Figure 6).

In 2008, Wagner *et al*.[48] applied in situ UV-vis spectroscopy for *in situ* monitoring and kinetic measurements of the generation of metal nanoparticles by borohydride reduction in silicon-glass micro-mixers. This approach allowed them to demonstrate that the size and size distribution of metal nanoparticles depend on the process parameters. Microfluidic devices with in situ UV-vis spectrometry are also used in the medical field to measure the solubility of powder for example. Recently, Peybernès *et al*.[49] presented a device made of PEEK (Polyether ether ketone) in order to generate saturated solutions. Their work enables to rapidly measure the solubility of a compound in different solvents with concentrations from *mg/ml* to hundreds of *mg/ml*.

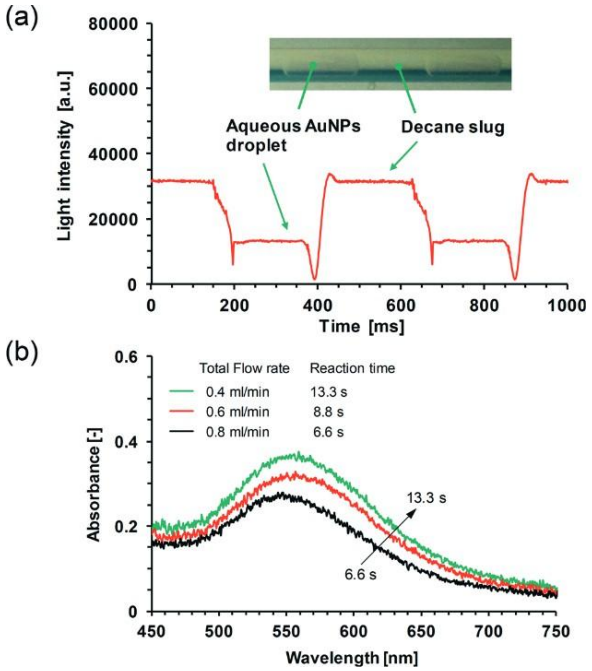

Figure 6: Online UV-vis monitoring of gold nanoparticles produced in a capillary micro-reactor. (a) UV-vis spectrum obtained in a cross-type flow-through cell at a light wave-length of *559 nm* and an integration time of *2 ms*. The inset shows an image of liquid–liquid segmented flow in the capillary micro-reactor. (b) UV-vis absorption spectra of the GNP solution in the cell (reproduced from ref. [47]. © The Royal Society of Chemistry 2013).

v. Infrared spectroscopy

Although optical microscopy allows for accessing critical information, spatial chemical information cannot be obtained through such approaches. Therefore, it is also critical to map the chemical composition of a fluid mixture for measuring kinetics in microfluidic devices. In this context, infrared spectrometry has been proven to be an effective non-invasive technique that can be coupled to microfluidics for *in situ* analysis. One could monitor the kinetics of a chemical reaction or a diffusion phenomenon, while it could also give access to the composition of different phases in a multiphasic flow and to solubility limits measurements. However, progress in term of microfabrication methods and materials along with devices development still need to be done, especially for high pressure applications. Materials traditionally used in the fabrication of microfluidic devices (glass, polydimethyl-siloxane (PDMS), borosilicate glass, *etc.*) do not exhibit transparency properties allowing performing Fourier transform infrared (FT-IR) characterization primarily due to IR absorption. To overcome this problem, Mid-IR wavelength transparent microdevices have been developed[50,51] to couple Mid-Infrared (Mid-IR) spectroscopy (wavelength between *3* and *50 μm*) with microfluidic devices. Therefore, such setups have been used for decades[52,50,53].

Barich *et al.*[51] presented an innovative fabrication method that allows the combination of PDMS with IR spectroscopy. Indeed, by using an IR transparent backbone such as CaF_2 and by keeping a total chip thickness under 200 *μm*, the authors were able to obtain IR compatibility for accessing important information on carbonyl, azide and nitrile vibrational modes. Others worked on the image optimization[54,55] or on the signal enhancement[56] to avoid any setup modification.

New Fourier transform infrared (FT-IR) spectrometers can also be coupled with microfluidics[57], as long as transparency issues are taken into account. They have the main advantages of improving the signal to noise ratio and of reducing the scanning time at all frequencies. Polshin *et al.*[58] reported the coupling of a FT-IR microscope with microfluidics for the label-free study of enzyme kinetics. By the mean of a Si-PDMS-CaF_2 microdevice (with only a *10 μm* PDMS layer thickness), they investigated the kinetics of the enzymatic reaction between D-glucose and glucose oxidase using Mid-IR spectroscopy. They also demonstrated the quantification of the spatial distribution of water and oil inside micro-channels based on their Mid-IR spectra (Figure 7). Such approaches can also be used into various different fields like chemistry[59], biology[60] and even pharmaceutical drug investigations[61].

Recently, in 2016, Perro *et al.*[62] wrote a review about combining microfluidics and FT-IR spectroscopy in order to obtain information on chemical processes. One of the main limitations of infrared spectroscopy is that it cannot be easily employed for aqueous media since water exhibits a strong absorption band in the *3000 – 3700 cm^{-1}* area due to the O-H stretching vibration.

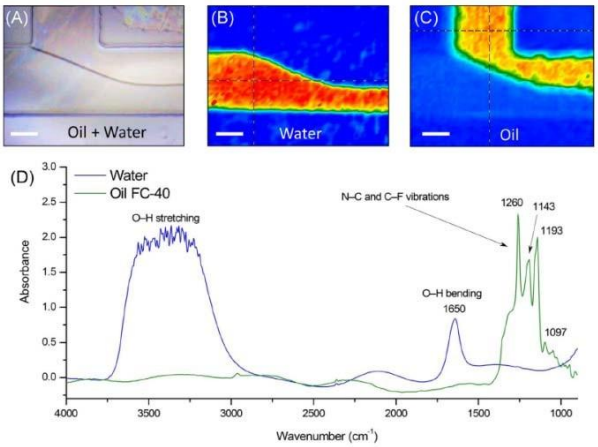

Figure 7: Vis (A) and FT-IR images of coflowing water (B) and oil (C) in a micro-channel. The scale bars represent *100 μm*. Mid-IR absorption spectrum of water and oil (D), extracted from the main and the second channel (at the cross of the two dashed lines) (Reproduced from ref. [58]. Copyright 2014 Elsevier B.V. All rights reserved).

vi. Raman spectroscopy

The local molecular fingerprint of the chemical composition of a fluid can be of interest to monitor diffusion and mixing phenomena. Coupling Raman spectroscopy and microfluidics offers that possibility. Raman microscopy is yet another advanced spectroscopy technique combining optical microscopy, laser excitation and spectrometry. It allows acquiring experimental data on the composition of organic and inorganic chemical compounds available in small quantities. Raman peaks can even give information about the local pressure of the system[63] like in the case of CO_2, in which the Fermi dyad shifts with pressure. As water is a weak Raman scatterer, this approach can be applied to obtain information about the chemical composition of aqueous

phases. Raman spectroscopy is therefore highly complementary to IR spectroscopy.

In 2010, Lin *et al.*[64] studied the temperature dependence of diffusion coefficients for the toluene/cyclohexane system in silicon-glass microdevices by the mean of a confocal Raman microscope. Using a Y-junction microfluidic chip, they monitored the diffusion of two fluids flowing side by side (Figure 8) and determined their interdiffusion coefficients.

However, they found the heating effect induced by the Raman laser to contribute abnormally to high diffusion coefficients values. In that case, they had to coat the channel bottom with a *200 nm* thick aluminum reflection film to eliminate this bias. In 2012, Liu *et al.*[65] studied the CO_2 solubility in water and brine using confocal Raman spectroscopy. One of their observations demonstrated that in segmented microflows, the equilibrium is reached in less than a minute. They operated under pressures ranging from *11* to *100 bar* and temperatures from *22* to *100 °C*.

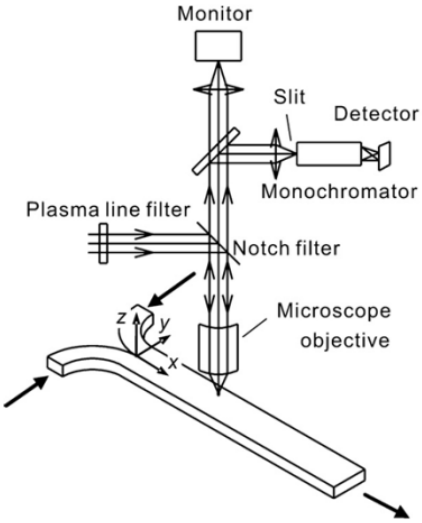

Figure 8: Schematic view of Raman measurements in a Y-junction microchannel. A Raman microscope was operated at hydro- and thermodynamic steady states (Reproduced from ref. [64]. Copyright 2010 Elsevier B.V. All rights reserved).

More recently, Luther *et al.*[66] worked on the determination of vapor-liquid equilibrium data using Raman spectroscopy on a segmented flow inside a capillary. In the studied conditions, they also determined the composition of the different phases at several positions after the mixing point (Figure 9).

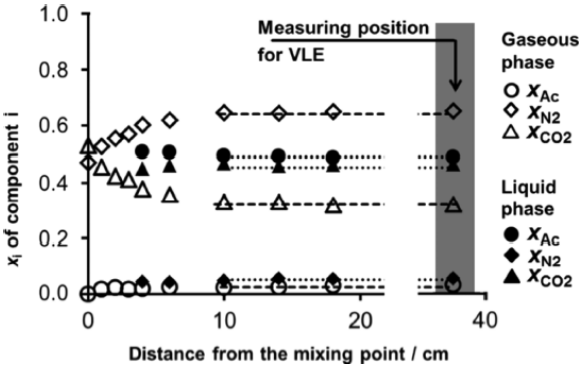

Figure 9: Equilibration process for the ternary system of CO_2, N_2, and acetone, showing the composition of the two phases with increasing distance to the mixing point in a capillary (Reproduced from ref. [66]. Copyright 2015, American Chemical Society).

Raman spectroscopy can also be used to characterize hydrate crystals and help understand hydrate formation conditions, which can cause serious damage in oil production. In 2017, *Chen et al.*[15] combined a silicon-Pyrex® microdevice with a Peltier thermoelectric cooling system (for temperature control), a CCD camera to monitor methane hydrate formation and propagation,

and Raman spectroscopy to confirm that they were actually observing hydrates and not ice. In their study, they also use Raman spectroscopy to monitor the hydrate density.

To summarize, microdevices implemented with *in situ* characterization are operational to perform thermodynamic properties determination at microscale. Label-free and non-intrusive measurements to access thermodynamic data on fluid systems are possible by adapting instruments and tools and by working on associated innovative approaches.

Strategies for accessing thermodynamic properties of fluids at small scales

In this section we will review microfluidic approaches developed for fast screening *in situ* characterization of viscosity and density, mass transfer and solubility, and phase equilibrium determination. We will focus on high pressure and high temperature microfluidic approaches and methodologies. Although some studies are not done on microfluidic devices capable of working under high pressure conditions, their approaches and methodologies could be applied for such devices. As already mentioned, *in situ* thermodynamic properties characterization instruments and methodologies have been developed to allow label-free non-intrusive *in situ* measurements on microfluidic devices. New challenges are to be faced in order to perform thermodynamic properties characterization under more realistic conditions (pressure and temperature of oil reservoirs for example).

Viscosity

Thermodynamic properties such as fluid viscosities can be measured using simple processes. The most common method reported in the literature is the co-flow method. The principle is to measure the position of the interface of two non-miscible fluids – the fluid of interest and a reference fluid of known viscosity – that flow in a laminar and parallel way in a microfluidic channel. Such devices generally have two inlets that meet at a T-junction (Figure 10 (c)). For a same flow rate, the fluid with a higher viscosity value will fill a higher volume in the channel due to its lower speed.
In their study, Guillot *et al.*[29] managed to determine the shape of the interface and therefore its exact position by using optical microscopy on a PDMS microfluidic chip. Indeed, different flow patterns can be observed depending on the flow rates and the viscosities of the two fluids. Once the position of the interface is measured and knowing the flow rates of the two liquids, the pressure drop in the microchannel and the viscosity of the fluid of interest can be computed. Note that the detection of the exact position of the interface can be challenging depending on its shape (Figure 10 (a) and (b)).
In order to overcome this issue, Kang *et al.*[67,68] developed a microfluidic design composed of two inlets and one hundred indicating channels leading to two distinct outlets. Two fluids are injected independently in the inlets (located in the centre of each circle on the schematic of Figure 11). The position of the interface is measured by simply counting the number of channels filled with a single fluid.

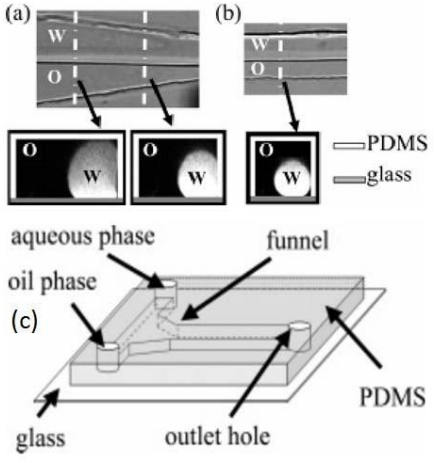

Figure 10: Cross-sectional picture of the parallel flow between hexadecane (O) and an aqueous phase with rhodamine (W) in a *100 μm* × *100 μm* microchannel. (a) Inside the funnel. (b) In the outlet channel. (c) Sketch of the microfluidic device (Reproduced from ref. [29]. Copyright 2006, American Chemical Society).

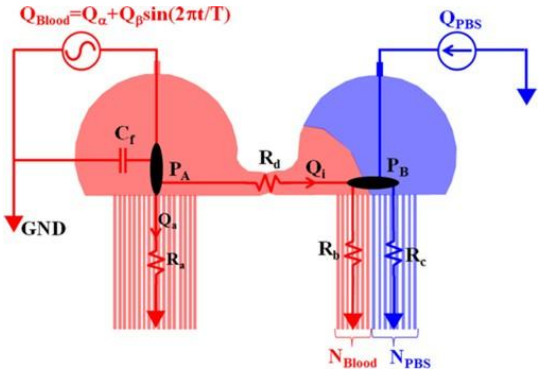

Figure 11: Schematic representation of the microfluidic device for viscosity measurements using a discrete fluidic circuit model. The path taken by the fluid depends on the hydrodynamic resistances. The position of the interface is measured by simply counting the number of channels filled with a single fluid (Reproduced from ref. [67], with the permission of AIP Publishing).

They also developed a two outlets device where flow rates ratio needs to be adjusted in order for a fluid to switch from one outlet to the other[69], which correspond to a specific viscosity value (Figure 12).

Using a stainless steel needle in a Teflon capillary, Lan *et al.*[70] worked on stable liquid/liquid annular co-laminar flows. By measuring the diameter of the inner phase (Figure 13) and by solving the Navier-Stokes equations, they were able to determine the viscosity of one fluid knowing the one of the other.

Taking advantage of new technologies available to the general public, Kim *et al.*[71] developed a hybrid system with a smartphone camera coupled with an objective lens and a Y-junction microfluidic device for viscosity measurement (Figure 14).

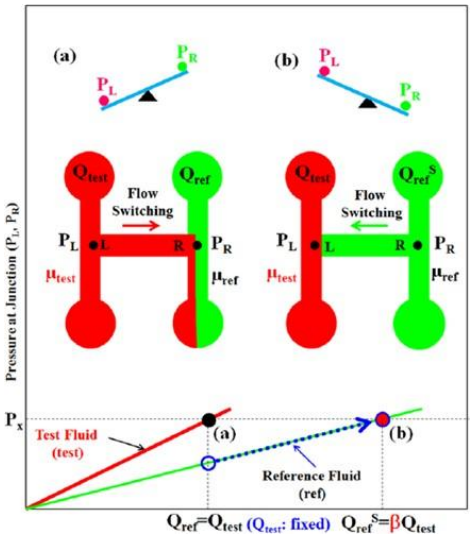

Figure 12: Proposed viscosity measurement method using fluidic flow switching in microfluidic channels based on hydrodynamic balancing with a label-free operation. Schematic diagram of the proposed method using a simple microfluidic device. (a) Silicone oil and (b) blood (Reproduced from ref. [69], with the permission of AIP Publishing).

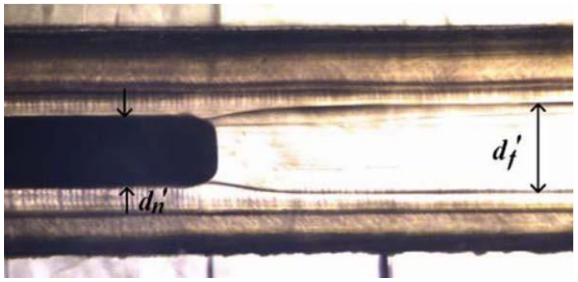

Figure 13: Image of a stainless steel needle coaxially inserted within a Teflon capillary, used to measure η^u_n and η^u_f. The inner phase comes from the stainless steel needle (Reproduced from ref. [70]. Copyright 2009, Springer-Verlag).

Their work is based on the same physical principle as discussed before. Even so, their approach offers great mobility for performing viscosity measurement on field and other analysis related to healthcare.

For example, commercial laboratory unit stations are also available using these methods like the FLUIDICAM RHEO from Formulaction Inc[72]. The device detects the interface position in a Y-junction to determine the viscosity of the fluid of interest.
Other microfluidic devices have been developed to measure fluid viscosity like a nanoliter capillary viscometer. By monitoring the capillary driven flow in a silicon-glass microfluidic chip (Figure 15), Srivastava *et al*.[73,74] were able to measure the viscosity of Newtonian and non-Newtonian fluids (given the condition that such fluids are monophasic) using a rearranged form of the Hagen-Poiseuille equation (as the pressure drop ΔP in a channel is a function of the hydrodynamic resistance R_K of the channel and the flow rate Q):

$$\Delta P = R_K Q$$

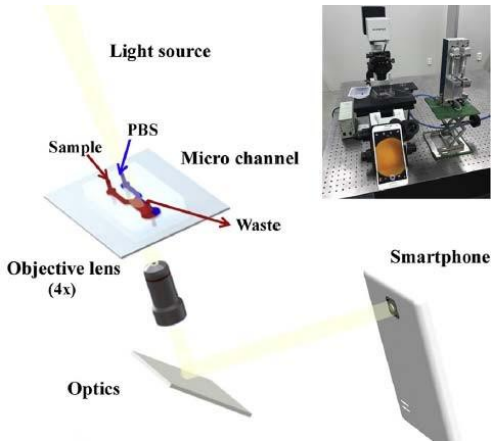

Figure 14: Schematics of the experimental setup composed of a smartphone, an objective lens and a microfluidic device to measure viscosity. A photograph of setup is inserted on the top right corner (Reproduced from ref. [71]. © 2018 Elsevier Ltd. All rights reserved.).

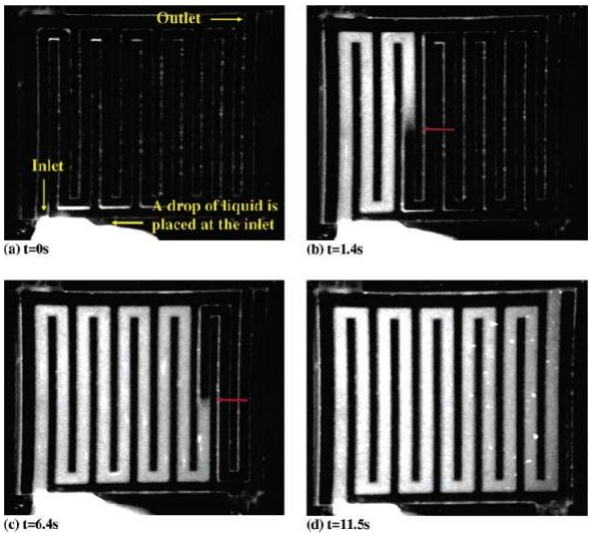

Figure 15: Snapshots from a test run on the micro-fabricated capillary viscometer. (a) *t = 0,* a pipet is used to place a drop of liquid at the inlet. (b-d) are snapshots of the liquid inside the channel as it moves toward the outlet. The red arrows indicate the advancing interface of the imbibing liquid (Reproduced from ref. [73]. Copyright 2005, American Chemical Society).

More sophisticated devices such as microelectromechanical systems (MEMS) also allow the measurement of the viscosity. Indeed, the vibration range of the vibrating cantilever of a MEMS depends of the fluid density surrounding that part. For instance, Cakmak *et al.*[75] presented a method for measuring blood plasma and serum viscosity using a micro cantilever-based MEMS sensor. Dehestru *et al.*[76] elaborated a microfluidic vibrating wire viscometer that works under high pressure and high temperature conditions. Srivastva *et al.*[77] integrated electrodes to their microfluidic devices in order to measure changes in the electrical conductivity and therefore viscosity. A self-powered microfluidic viscometer has been developed by Wang *et al.*[78], the working principle of such a device is based on the piezoelectric energy harvesting from flowing droplets.
Table 1 gives a comparison of the different viscosity ranges measured in the studies detailed above, depending on their approach.

Table 1: Summary of some microfluidic approaches for viscosity measurements

Reference	Viscosity range of the experiment	Shear rate (s^{-1})	Geometry
Guillot *et al.*[29]	*2 mPa.s* to *70 Pa.s*	*0.2* to *2000*	T-junction
Kang *et al.*[67,68,69]	Blood, N/A	N/A	Co-flow and hydrodynamic resistance
Lan *et al.*[70]	*0.6* to *40 mPa.s*	N/A	Annular co-flow
Kim *et al.*[71]	*1.5* to *130 mPa.s*	Up to *5000*	Y-junction
Fluidicam Rheo[72]	*0.1 mPa.s* to *200 Pa.s*	*100* to 10^5	Y-junction

Density

Density measurements using microfluidics is more challenging. Indeed, this property appears in the inertial forces. Since the flow inside a microfluidic channel is laminar, inertial forces are very small compared to viscous forces, therefore, observing them is challenging in conventional microfluidic systems.

However, Pinho *et al.*[79] showed they can simultaneously determine the viscosity and the density of a fluid mixture by measuring the pressure drop between the inlet and the outlet of a flow in a capillary. The only condition for this process to stay in a reasonable range of precision, the pressure drop should not increase too much to significantly change the fluid mixture thermophysical properties. Indeed, the density and the viscosity will change with the pressure along the tubing due to the pressure drop. The pressure drop ΔP can be expressed by the Hagen-Poiseuille equation:

$$\Delta P = 16 Q^2 \rho \frac{\mu}{A^4} \left(\frac{L}{\bar{P}} \right) \quad (1)$$

Where Q is the mass flow, μ is the fluid dynamic viscosity, A is the cross-section, L is the length between the two spots where the pressure is measured, the fluid density ρ appears in the molecular mass M ($M = \rho R T (P^{-1})$), I_p is the polar moment of inertia which depends on the geometry of the channel cross-section, Z is the compressibility factor, R is the ideal gas constant, T is the temperature, $\bar{P}$ is the average pressure and P is the pressure. The process has been applied to pure fluids (CO_2 an N_2) and then to mixtures (cyclohexane + CO_2 and CO_2 + H_2). From these pressure losses, the density and the viscosity were consequently determined. Figure 16 shows the experimental data compared with the NIST data base or calculated using PR78 equation of state. This process is appropriate to determine densities of (i) monophasic and homogenous fluids (ii) in a laminar flow. However, for small viscosity values, one needs to improve the uncertainty concerning the measurement of the pressure drop.

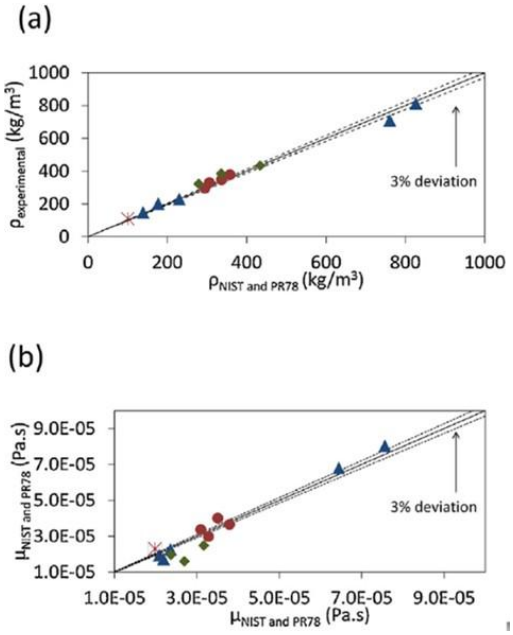

Figure 16: Parity graphics for density (a) and viscosity (b) of pure compounds (ΔCO_2 and $*N_2$) and mixtures (•CYC + CO_2 and ♦CO_2 + H_2) at homogeneous experimental conditions (Reproduced from ref. [79]. Copyright 2015 Elsevier B.V. All rights reserved).

MEMSs have also been developed to perform density measurements in parallel with viscosity measurements. Such devices are based on the resonant frequency of objects such as cantilevers[80], silicon beams[24], micro-plate[23] or suspended micro-channel resonators[81]. The resonant frequency of these vibrating objects depends on the hydrodynamic forces applied on them. Since these forces are a function of both viscosity and density, these two thermodynamic properties can be measured by monitoring the resonant frequencies.

Table 2 gives a comparison of the different density ranges measured in some of the studies detailed above, depending on their approach. The approach developed by Pinho *et al.*[79] is the only non-MEMS based study, however the mass flow rates of the different compounds of the fluid mixture need to be known.

Table 2: Summary of some microfluidic approaches for density measurements

Reference	Density range ($kg.m^{-3}$)	Uncertainty	Approach
Pinho *et al.*[79]	*111* to *813*	*4 %*	ΔP measurement
Cakmak *et al.*[80]	*995* to *1150*	*< 3 %*	MEMS cantilever
Harrison *et al.*[23]	*600* to *1500*	N/A	MEMS vibrating plate

Mass transfer and solubility measurement strategies at micro-scale

In microfluidics, mixing several miscible phases is mainly achieved by molecular diffusion because most of the time, flows are laminar. The time τ_d a molecule takes to diffuse on a distance l can be roughly estimated by:

$$\tau_d = \frac{l^2}{D}$$

with D the molecular diffusion coefficient. Having a homogenous sample across the system can take a time that can become non-negligible compared to convection times. However, the advantage of working on such small distances is that molecular diffusion is the only reason for mixing. Therefore, diffusion coefficients of a system can be determined by knowing the distance of complete mixing.

A T sensor (Figure 17) is a microfluidic device that allows to monitor optically the diffusion of components from several input fluid streams. Therefore, analyte concentrations can be measured on a continuous basis using fluorescence, which gives a cartography of concentrations and allows the back-calculation of the diffusion.

In 1999, Kamholz *et al.*[26] presented a method for determining diffusion coefficients by interpreting T-sensor experiments through a model.

Later on, they extended their model by quantifying the time-dependent evolution of analyte distribution[82]. They managed to get an accurate representation of the shape of the diffusion region. By quantifying the importance of the velocity profile on the distribution of analytes, this last study brings an important improvement in the precision of the measurements.

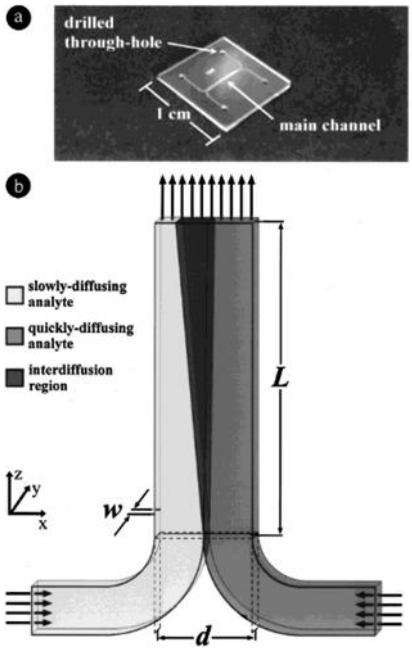

Figure 17: (a) Photograph of a silicon-Pyrex® micro-fabricated device. For operation as a T-sensor, two inputs and one output are used. (b) Schematic representation of flow in the T-sensor with two input fluids, each containing one diffusing species. The flow is at steady state, projecting the interdiffusion along the length of the channel (Reproduced from ref. [26]. Copyright 1999, American Chemical Society).

Over time, several models have been developed[83], Broboana *et al.*[35] even took into account and analyzed effects that occur during the non-stationary dynamical process like the "butterfly effect" (asymmetry in concentration due to the parabolic velocity in the channel).

The following year, in 2002, Culbertson *et al.*[34] compared four methods to measure diffusion coefficients using rhodamine 6G as analyte. Their results were all within the experimental error bar of one another and previously reported values except for one method where the diffusion coefficient measured is *11 %* higher. This gap can be explained by the analyte-wall interactions or their accuracy in measuring the chip temperature. They also concluded that static methods can give acceptable results as long as the equilibration time for adsorption-desorption processes remains small versus the measurement time.

During the past years, numerous works were done on the optimization of methods to study the diffusion process through microfluidics[25,84,85,86]. Focusing on getting the best measurement conditions to minimize experimental uncertainties, Häusler *et al.*[87], inspired by the work of Franceschini *et al.*[88], started by developing a model that gave them the theoretical optimal experimental designs of a microfluidic H-cell (Figure 18). Then, they tested these designs based on the optimal Fourier number (it represents a dimensionless contact time, defined as $\frac{Dt}{S^2}$ with *D* the diffusion coefficient, *t* the average residence time in the channel and S the channel half width). Their results were consistent with the literature values and came to the conclusion that the ratio (height over width) of a channel is the most important parameter to master in order to minimize uncertainties on diffusion coefficient measurements. Other studies like the one from Wolff *et al.*[89] were about finding the optimal geometries to measure diffusion coefficients, but not limited to micro scale.

Getting access to diffusion coefficients in fluids systems is critical. Indeed, in order to measure miscibility using microfluidic devices, one needs to be certain that the diffusion process is over. In some cases, chemical reactions also need to be taken into account[30] but this is not the scope of this review. When working with a non-reactive system, microfluidics can be a high throughput experimentation tool that can be used from biology[90,91] to physics and CO_2 applications. With progress made in the fabrication of microdevices over the past decades, studies concerning oil extraction and CO_2 storage[92] problematics can be conducted under high pressure conditions. In 2017, Bao *et al.*[93] wrote a critical review where they summarized microfluidic phase characterization methods for CO_2, oil and gas. Among the studies on CO_2 solubility[39,94,95,96,97], one simple way to measure CO_2 solubility in solvents concerns the monitoring of CO_2 bubbles dissolution by image processing[94,96]. Abolhasani *et al.*[94] monitored the volume of a bubble in a microfluidic channel to determine the quantity of CO_2 dissolved in a solvent (Figure 19).

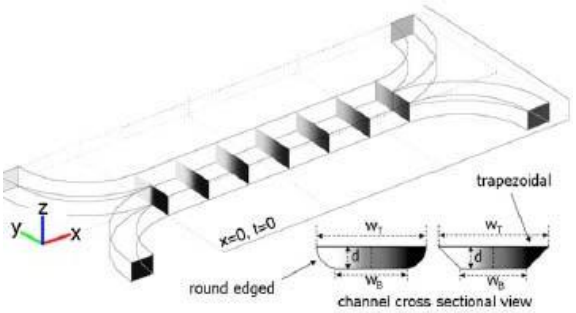

Figure 18: Schematic representation of the H-cell. Gray intensity represents concentration change during the diffusion process. Such models were used to give the optimal experimental design (Reproduced from ref. [87]. Copyright 2012 Elsevier Ltd. All rights reserved).

Such a method can combine fast and accurate measurements when working with gases exhibiting a low density. However, when the dissolved fluid is liquid, the solvent is rapidly saturated and the volume variation of a droplet is not quantifiable or the variation remains in the measurement uncertainty. To address this problem, Liu *et al.*[65] used a Raman Spectroscopy. They reported an accurate method to quantify dissolved carbon dioxide in water and salted water using a microfluidic systems probed by Raman spectroscopy. Other methods have been developed over the years. In 2013, Fadaei *et al.*[98] have presented a microfluidic approach to measure toluene diffusivity in Athabasca bitumen by imaging transmitted light profiles over time (Figure 20).

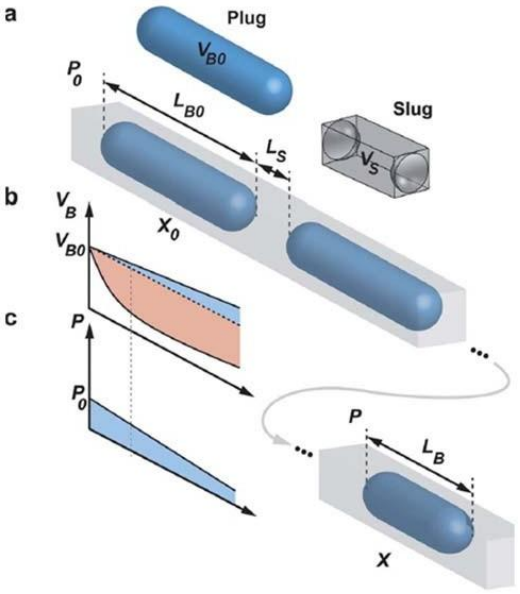

Figure 19: (a) Schematic drawing of a CO_2 plug shrinkage in a segmented flow. (b) The net plug volume reduction (highlighted in red colour) that results from the competing effects of pressure drop and gas dissolution is schematically shown. Plugs isothermally expand due to the decreasing pressure (highlighted in blue colour). (c) Pressure profile along the flow direction (Reproduced from ref. [94]. Copyright 2012 RSC publications).

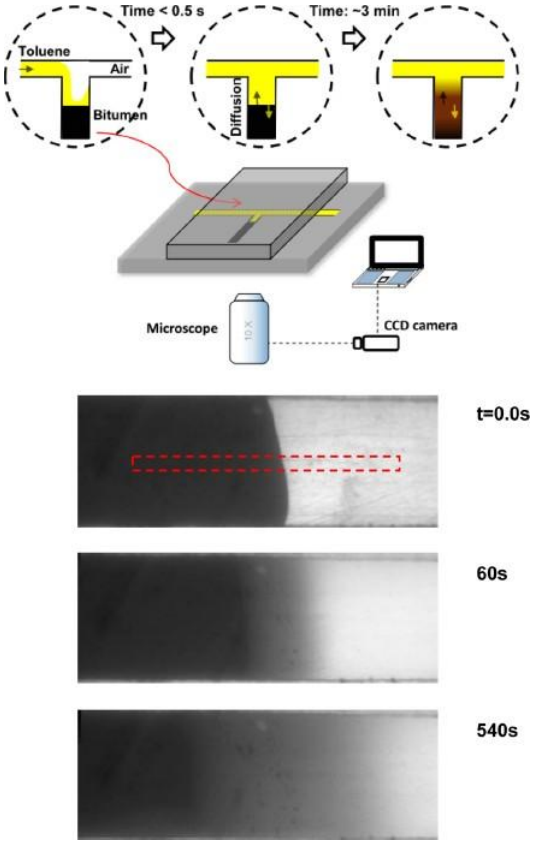

Figure 20: Schematic representation of the experimental microfluidics-based setup for toluene–bitumen mutual diffusion coefficient measurement. The magnified image shows the section of the channel near the interface. Top: before toluene injection,

where the rest of the system is filled with air. Middle and bottom: Toluene–bitumen mutual diffusion in the microchannel (Reproduced from ref. [98]. Copyright 2013, American Chemical Society).

In 2016, Sieben *et al*.[99] worked on the evaluation of the solubility of asphaltenes in crude oil. The asphaltenes precipitation was monitored by the change in optical absorbance for each chosen solvent volume fraction (Figure 21).

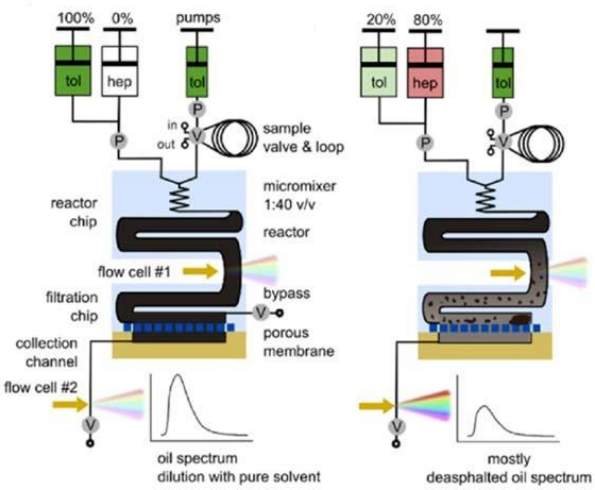

Figure 21: Conceptual diagram for measuring asphaltene solubility in solvent mixtures using an automated microfluidic apparatus. The symbols V and P represent valves and pressure sensors. The optical absorbance is a function of the asphalten concentration (Reproduced from ref. [99]. Copyright 2016, American Chemical Society).

More recently, in 2017, Talebi *et al*.[36] demonstrated a microfluidic approach to determine both the solubility and diffusivity of propane in bitumen by monitoring the swelling of bitumen in a microfluidic PVT cell using fluorescence. The next year, in 2018, Sharbatian *et al.*[37] expanded this approach by redesigning the microfluidic chip (Figure 22) to enable several measurements on the same experimentation. They worked on a CO_2-crude oil system to determine mutual solubilities and diffusivities, along with the measurement of the minimum miscibility pressure, the extraction pressure and the contact angle.

In order to have a better knowledge about mass transfer occurring across interfaces, Pinho and Hartman[100] developed a new microfluidic device. By trapping volumes of a non-polar liquid fluid (here toluene) in a water flow (Figure 23), the composition of the interface was characterized using Raman spectroscopy and different zones (toluene bulk, mixing zone and water bulk) were identified. Oppositely to the literature, they found, in their experimental conditions (*2* to *20 µl/min* in their *800x800x500 μm^3* trap), the flow rate to have no influence on the thickness of the interface. This method could be exploited to study the relation between mass transport and the interface thickness and also to analyze concentration profiles in different zones of the chip during the same experiment.

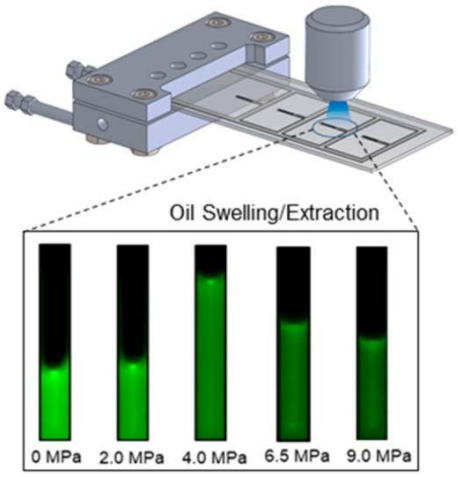

Figure 22: Microfluidic platform for CO_2–oil phase behavior; Schematic view of a microfluidic setup combined with fluorescence microscopy; and typical oil swelling and extraction inside the micro-PVT channel (Reproduced from ref. [37]. Copyright © 2018, American Chemical Society).

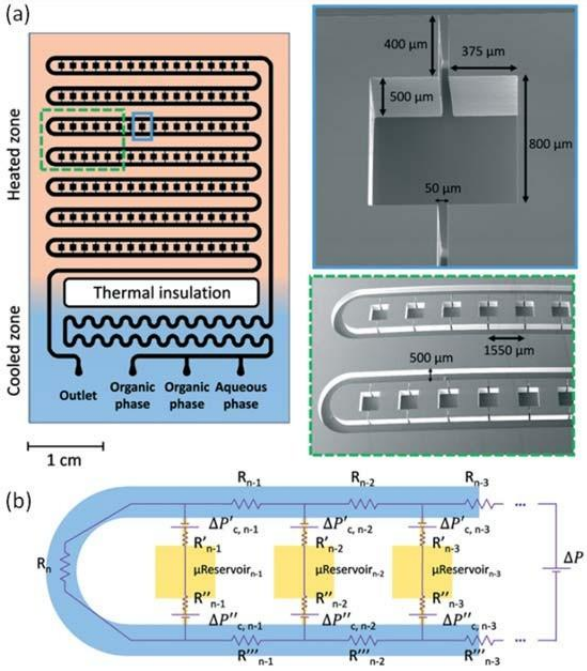

Figure 23: (a) Microfluidic semi-flow device. (b) Scheme of a hydrophilic phase injection into a microchannel filled with a hydrophobic phase and electrical analogue for its stationary state (Reproduced from ref. [100]. Copyright 2017 RSC publications).

A summary of some approaches described above is given in Table 3. Microfluidics coupled with in situ characterization techniques enables to obtain critical information around interfaces, and therefore, it is a powerful tool to work on mass transfer characterization.

Table 3: Summary of some microfluidic approaches to measure mass transfer related properties

Reference	Property	Property range	Approach
Culbertson	Diffusion coefficient	10^{-6}	Static & dynamic

et al.[34]	($m^2.s^{-1}$)		analyte monitoring
Häusler *et al.*[87]	Diffusion coefficient ($m^2.s^{-1}$)	*1.18 - 3.4 .10^{-9}*	Conductimetry
Liu *et al.*[65]	Diffusion coefficient ($m^2.s^{-1}$)	*10^{-9}*	Raman spectrometry on a segmented flow
Talebi *et al.*[36]	Diffusion coefficient ($m^2.s^{-1}$)	*10^{-10}* to *10^{-8}*	Fluorescence
Liu *et al.*[65]	Solubility of CO_2 in water and brine (*mol/mol*)	*0.003* to *0.023*	Raman spectrometry on a segmented flow
Abolhasani *et al.*[94]	Volumetric vapor-liquid mass transfer coefficient $k_L a$ (s^{-1})	*5* to *30*	Optical detection on a segmented flow
Sauzade *et al.*[96]	Dissolution coefficient k_D of CO_2 in silicone oil ($g.m^{-2}.s^{-1}.atm^{-1}$)	*0.8* to *100*	Optical detection on a segmented flow
Talebi *et al.*[36]	Solubility of propane in bitumen ($kg.m^{-3}$)	*2.5* to *5.1*	Fluorescence

Liquid-liquid extraction

The need for separating solutes in analytical chemistry or to recover products in chemical engineering has generated numerous microfluidic studies on liquid-liquid extraction[101,102,103]. This interest on microfluidics is based on the simple principle that at small scale, extraction is enhanced due to small length transfer and high interfacial areas.

Under high pressure and high temperature conditions, efficient microextractions have been demonstrated and quantified in supercritical CO_2. Assman *et al.*[104] used a segmented flow for vanillin continuous extraction in a microdevice and measured distribution coefficients. Segmented flows, allowing good interfacial exchanges, are flow regimes favored in that case, due to the small viscosity of supercritical CO_2[105]. The possibility to investigate steps involved in extraction processes illustrated by a supercritical fluid extraction of emulsions is discussed by Luther *et al.*[106].

Microfluidic tools under high pressure and high temperature conditions are fast and efficient for separation processes. They open new ways for studies and screening, but lack of high throughput: device parallelization may be necessary for production purposes[103,106].

Phase equilibria

Many macroscopic approaches have been developed to study the phase behavior of fluid mixtures[107,108,109,110] but lately, microfluidics became a powerful tool in this domain. As mentioned earlier, phase equilibria are rapidly reached in microfluidic devices and accessing thermodynamic diagrams of pure fluids or fluid mixtures can take less than a day.

Phase diagrams and envelope diagrams are often obtained using silicon-Pyrex® microfluidic devices as they allow working under high pressure and high temperature conditions (up to *300 bar* and *400 °C*)[5]. Moreover, the glass cover provides an optical access to phase and transport behavior in micro-channels. In 2012 and 2014 Mostowfi *et al.*[2,111] presented two microfluidic PVT devices for analyzing phase diagrams of gas-liquid systems. Their setup[2] consists in injecting a fluid mixture (selected to represent the phase behavior of typical black oils), initially liquid, in a long serpentine microchannel to generate an isothermal pressure gradient (at room temperature). When the pressure in the channel decreases under the bubble point, the first bubbles nucleate (Figure 24). These conditions refer to a transition point on the phase diagram of the mixture. Such a device is a breakthrough in petroleum engineering because it allows working under reservoir conditions and it reduces the measurement time of thermodynamic properties from hours to minutes. This method can only be used to detect the bubble point of a pure compound or a fluid mixture but does not allow the detection of the dew point to determine the full phase envelop of a mixture and can only be carried out in a continuous flow mode.

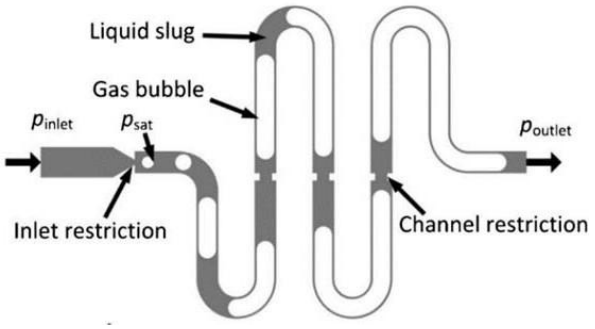

Figure 24: The concept of the microfluidic technique for phase behavior determination. A saturated gas–liquid mixture is injected at high pressure (greater than the bubble point) into the channel. Once the pressure drops below the one of the bubble point (at the restriction), a two-phase slug flow is formed (Reproduced from ref. [2]. Copyright 2012 RSC publications).

To overcome this challenge, Pinho *et al.*[13] developed a silicon-Pyrex® microfluidic device imitating a PVT cell in a dynamic stop flow concept. Phase transitions like bubble and dew points are optically detected. The fluid mixture is at equilibrium within the microsystem, and then the temperature is increased or decreased under isobaric conditions. The bubble point corresponds to the temperature at a given pressure for which the first bubble starts nucleating in the fluid (Figure 25). The dew point corresponds to the temperature at a given pressure for which the last bubble disappears in the fluid. This method is repeated at higher pressures until the maxcondembar is reached. This point corresponds to the maximum pressure value on the P-T envelope. Under isochoric conditions (stop flow mode), the pressure is linked to the temperature variations, which is a lack of liberty in the setting of the conditions. Working under a continuous flow mode allows a better setting of the fluids conditions but leads to a slight uncertainty on the pressure measurement due to the pressure loss between the inlet and the outlet of the chip.

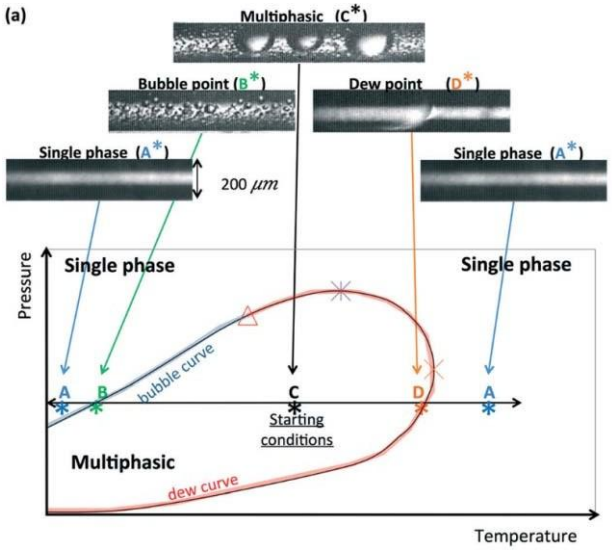

Figure 25: General loop method for building a P–T phase diagram through bubble and dew point detection and phase envelope construction. The bubble and dew points were determined by increasing or decreasing the temperature from the initial conditions under isobaric conditions (Reproduced from ref. [13]. Copyright 2014 RSC publications).

Song *et al.*[14] also developed a smart microfluidic device to optically determine the dew point conditions for CO_2 with impurities. A more complex device has been elaborated by Bao *et al.*[22] where bubble and dew points are detected using optical thin-film interference in a PVT cell.

Although these approaches are much quicker than at the macroscopic scale, only a single pressure-temperature point can be measured at once. This is a restricting factor but further research has allowed observing a phase diagram directly on the chip.

Bao and al.[18] developed a device allowing the direct observation and measurement of the full pressure-temperature phase

diagram of a pure fluid. The micro-chip is made of silicon sealed with glass. The areas of interest are located in the one hundred horizontal dead-end channels. Each of these channels has one hundred orthogonally connected microwells in order to have a better vision of the transition points. Each channel is connected on the left side to a vertical serpentine channel acting as a fluidic resistance. This channel provides an elevated hydraulic resistance so that when the fluid flows through the micro-channel, a vertical pressure gradient is induced due to the linear pressure drop. A temperature gradient is then applied horizontally. The bubble points can therefore be observed and be determined in the dead-end channels. When precise conditions have been reached, the vapor state, liquid state and the supercritical region can be observed simultaneously. The setup allows the distinguishing of the liquid-vapor saturation line all the way to the critical point on the chip (Figure 26).

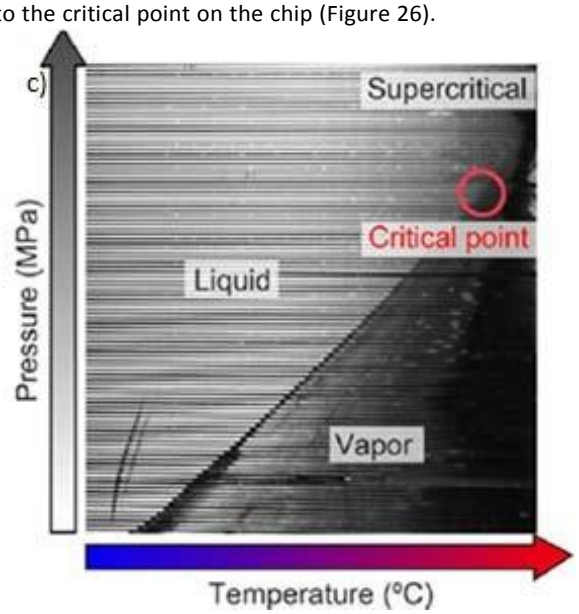

Figure 26: Measurement of the pressure–temperature phase diagram of pure CO_2. Phase-mapping device in operation, with liquid, vapor, and supercritical regions visualized (Reproduced from ref. [18]. Copyright 2016, American Chemical Society).

This method only allows the study of pure compounds. To overcome this issue, Xu *et al.*[19] extended the system and developed a new methodology working with a piston fluid. This new tool enables the visualization of the entire P-T phase envelope of a fluid mixture. The fluid of interest is compressed in one thousand microfluidic chambers, each isolated by the piston fluid (Figure 27). The piston fluid must be immiscible under any test condition with the fluid system. A pressure gradient is applied using the same principle as Bao et al.[18]. Therefore, each chamber represents the thermodynamic steady-state of the system at a given condition of pressure and temperature. Although this new method is a step forward in the high throughput experimentation, it is limited in the fact that the device must be filled with a fluid at the state of vapor to be compressed into the chambers. Moreover there is the difficulty to change the fluid composition (the microfluidic chambers need to be emptied). In addition, finding a suitable piston fluid could be difficult especially, when supercritical and subcritical conditions are reached on the same experiment.

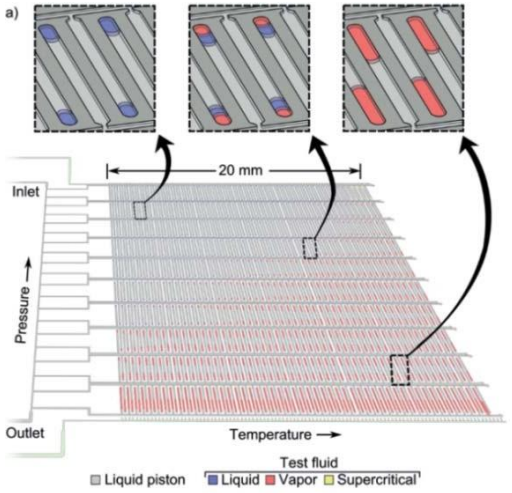

Figure 27: Schematics of the rapid pressure–temperature phase mapping device for fluid mixtures. The 1000 chambers are isolated and pressurized by a piston fluid. They represent the thermodynamic equilibrium state of the fluid system, each at a given pressure and a given temperature (Reproduced from ref. [19]. Copyright 2017, Wiley-VCH Verlag GmbH & Co.).

A MEMS-based microfluidic device has been developed by Sullivan *et al*.[112] to measure the bubble point of an unknown fluid. The glass-silicon-glass sandwich structure has a built in heater electrode generating short heat pulses. The heater electrode is followed by a detector electrode to increase the detection speed and sensitivity. The thermal pulses allow a bubble nucleation and the bubble size is then monitored.

An overview of the methods described above is given in Table 4, as well as the operating conditions.

Table 4: Summary of some microfluidic approaches for phase equilibria determination. All microfluidic devices are silicon-glass based, only Song et al.[14] is glass-glass based.

Reference	Property	Experimental conditions	Approach
Mostowfi et al.[2]	Bubble point	*5 - 45 bar* Room temperature	Optical detection
Mostowfi et al.[2]	Liquid-vapor phase volume distribution	*5 - 45 bar* Room temperature	Image processing
Molla et al.[111]	Bubble point	Up to *860 bar* Room temperature to *150 °C*	Optical detection
Molla et al.[111]	Liquid-vapor phase volume distribution	Up to *860 bar* Up to *150 °C*	Image processing
Pinho et al.[13]	P-T phase envelope of fluid mixtures	Up to 140 bar Up to 300 °C	Optical detection
Song et al.[14]	Dew point	Up to 130 bar Up to 50 °C	Optical detection
Bao et al.[18]	P-T vapor-liquid saturation line	Up to 80 bar Up to 38 °C	Optical detection
Xu et al.[19]	P-T phase envelope and liquid-vapor phase volume distribution	Up to 70 bar Up to 90 °C	Image processing

Conclusion, challenges and opportunities

Microfluidics is commonly chosen for its main advantage to minimize the experimentation time. Especially under high pressure and high temperature conditions, microfluidic phase characterization is of growing interest. Indeed, progress achieved in manufacturing techniques are now allowing to access critical conditions and to adapt microdevices and *in situ* characterization instruments to be compatible with each other.

Thermodynamic properties characterization using microfluidic devices has been developed over the past decades. Recent progresses made in this field are now allowing to perform label-free and non-intrusive *in situ* characterization. To that end, characterization methods as well as microfluidic devices need to be adapted to be compatible. Measurements are done rapidly with very small quantities of fluids. Research under high pressure and high temperature conditions is now accessible with non-complex-heavy experimental setups. Indeed, for microfluidic devices to keep their good performances under such conditions, materials and methodologies need to be thoroughly selected, which implies limitations in terms of micromanufacturing flexibility. Thermodynamic properties such as viscosity, density, diffusion coefficient, solubility and phase equilibrium can be characterized directly on chip. To this purpose, tools usually employed at macroscopic scale have been improved to fulfill the specific conditions of high pressure and high temperature microfluidics without interfering with the measurement itself. Viscosity can be measured by studying co-flows in microfluidic T-junctions or in capillaries within one another. Density measurement is more challenging and typically requires the use of MEMS if the fluid is of unknown composition. Diffusion coefficient and solubility determination is achieved by monitoring the mass transfer between several phases in microchannels. Complete phase equilibria can also be determined by the optical detection of transition points in micro-reactors. Recent methodologies allow accessing a wide spectrum of experimental conditions (pressure and temperature) in one experiment, *i.e.* to perform high throughput experimentation. All these methods remain challenging under high pressure and high temperature conditions. New devices could allow widening even more the scope of experimental conditions to meet new application fields. One interesting way (aside from inventing new micro-chips) is to work on an even smaller scale. Nanofluidics is rising [113,114] and can be a lead to energy applications for example (such as oil extraction in nanoporous systems). In any event, by working on innovative designs and methodologies, opportunities are to be seized and important progresses are to be made to access multi-properties characterization and to perform high throughput experimentation. With an increasing demand in efficiency and a trend in miniaturization, the study of microfluidic approaches for *in situ* characterization of thermodynamic properties is burgeoning and very promising.

Conflicts of interest

The authors declare no conflicts of interest.

Acknowledgements

The authors acknowledge support from IFPEN, ICMCB CNRS and the Région Aquitaine for financial support. This work has received funding from the European Research Council (ERC) under the European Union's Horizon 2020 research and innovation program (Grant Agreement No. 725100, project BIG MAC).

References

1 T. H. Ahmed, *Equations of state and PVT analysis. Applications for improved reservoir modeling*, Gulf Professional Publishing, Amsterdam, 2017.
2 F. Mostowfi, S. Molla and P. Tabeling, *Lab on a chip*, 2012, **12**, 4381–4387.
3 R. Fisher, M. K. Shah, D. Eskin, K. Schmidt, A. Singh, S. Molla and F. Mostowfi, *Lab on a chip*, 2013, **13**, 2623–2633.
4 D. Eskin and F. Mostowfi, *International Journal of Heat and Fluid Flow*, 2012, **33**, 147–155.
5 S. Marre, A. Adamo, S. Basak, C. Aymonier and K. F. Jensen, *Ind. Eng. Chem. Res.*, 2010, **49**, 11310–11320.
6 A. Michels and R. O. Gibson, *The Royal Society*, 1931, 288–307.
7 F. Zhang, A. Erriguible, T. Gavoille, M. T. Timko and S. Marre, *Phys. Rev. Fluids*, 2018, **3**.
8 S. Marre, Y. Roig and C. Aymonier, *The Journal of Supercritical Fluids*, 2012, **66**, 251–264.
9 R. Knitter, D. Gohring, P. Risthaus and J. Haubelt, *Microsystem Technologies*, 2001, **7**, 85–90.
10 C. Iliescu, B. Chen and J. Miao, *Sensors and Actuators A: Physical*, 2008, **143**, 154–161.
11 R. M. Tiggelaar, F. Benito-López, D. C. Hermes, H. Rathgen, R. J.M. Egberink, F. G. Mugele, D. N. Reinhoudt, A. van den Berg, W. Verboom and H. J.G.E. Gardeniers, *Chemical Engineering Journal*, 2007, **131**, 163–170.
12 V. Miralles, A. Huerre, F. Malloggi and M.-C. Jullien, *Diagnostics (Basel, Switzerland)*, 2013, **3**, 33–67.
13 B. Pinho, S. Girardon, F. Bazer-Bachi, G. Bergeot, S. Marre and C. Aymonier, *Lab on a chip*, 2014, **14**, 3843–3849.
14 W. Song, H. Fadaei and D. Sinton, *Environmental science & technology*, 2014, **48**, 3567–3574.
15 W. Chen, B. Pinho and R. L. Hartman, *Lab on a chip*, 2017, **17**, 3051–3060.
16 Alex I.K. Lao, Thomas M.H. Lee, I-Ming Hsing, Nancy Y. Ip, *Sensors and Actuators A: Physical*, 2000, **84**, 11–17.

17 K. J. Shaw, P. T. Docker, J. V. Yelland, C. E. Dyer, J. Greenman, G. M. Greenway and S. J. Haswell, *Lab on a chip*, 2010, **10**, 1725–1728.
18 B. Bao, J. Riordon, Y. Xu, H. Li and D. Sinton, *Analytical chemistry*, 2016, **88**, 6986–6989.
19 Y. Xu, J. Riordon, X. Cheng, B. Bao and D. Sinton, *Angewandte Chemie (International ed. in English)*, 2017, **56**, 13962–13967.
20 M. Andersson, J. Ek, L. Hedman, F. Johansson, V. Sehlstedt, J. Stocklassa, P. Snögren, V. Pettersson, J. Larsson, O. Vizuete, K. Hjort and L. Klintberg, *Journal of Micromechanics and Microengineering*, 2016, **27**.
21 M. Andersson, K. Svensson, L. Klintberg and K. Hjort, *Analytical chemistry*, 2018, **90**, 12601–12608.
22 B. Bao, H. Fadaei and D. Sinton, *Sensors and Actuators B: Chemical*, 2015, **207**, 640–649.
23 C. Harrison, A. Fornari, H. Chen, S. Ryu, A. Goodwin, K. Hsu, F. Marty and B. Mercier, in SPIE, 2007, 64650U.
24 I. Etchart, H. Chen, P. Dryden, J. Jundt, C. Harrison, K. Hsu, F. Marty and B. Mercier, *Sensors and Actuators A: Physical*, 2008, **141**, 266–275.
25 C. Synovec, *Talanta*, 2002, **58**, 551–560.
26 A. E. Kamholz, B. H. Weigl, B. A. Finlayson and P. Yager, *Anal. Chem.*, 1999, **71**, 5340–5347.
27 J. T. Cabral and S. D. Hudson, *Lab on a chip*, 2006, **6**, 427–436.
28 J. H. Xu, S. W. Li, W. J. Lan and G. S. Luo, *Langmuir : the ACS journal of surfaces and colloids*, 2008, **24**, 11287–11292.
29 P. Guillot, P. Panizza, J.-B. Salmon, M. Joanicot, A. Colin, C.-H. Bruneau and T. Colin, *Langmuir : the ACS journal of surfaces and colloids*, 2006, **22**, 6438–6445.
30 C. Zhu, C. Li, X. Gao, Y. Ma and D. Liu, *International Journal of Heat and Mass Transfer*, 2014, **73**, 492–499.
31 Martinez de Baños, Maria Lourdes, O. Carrier, P. Bouriat and D. Broseta, *Chemical Engineering Science*, 2015, **123**, 564–572.
32 J.-W. Jung and J. C. Santamarina, *Journal of Crystal Growth*, 2012, **345**, 61–68.
33 J.-C. Baret, O. J. Miller, V. Taly, M. Ryckelynck, A. El-Harrak, L. Frenz, C. Rick, M. L. Samuels, J. B. Hutchison, J. J. Agresti, D. R. Link, D. A. Weitz and A. D. Griffiths, *Lab on a chip*, 2009, **9**, 1850–1858.
34 C. Culbertson, *Talanta*, 2002, **56**, 365–373.
35 D. Broboana, C. Mihai Balan, T. Wohland and C. Balan, *Chemical Engineering Science*, 2011, **66**, 1962–1972.
36 S. Talebi, A. Abedini, P. Lele, A. Guerrero and D. Sinton, *Fuel*, 2017, **210**, 23–31.
37 A. Sharbatian, A. Abedini, Z. Qi and D. Sinton, *Analytical chemistry*, 2018, **90**, 2461–2467.
38 A. Banerjee, Y. Shuai, R. Dixit, I. Papautsky and D. Klotzkin, *Journal of Luminescence*, 2010, **130**, 1095–1100.
39 P. Nguyen, D. Mohaddes, J. Riordon, H. Fadaei, P. Lele and D. Sinton, *Analytical chemistry*, 2015, **87**, 3160–3164.
40 S. Kuhn and K. F. Jensen, *Ind. Eng. Chem. Res.*, 2011, **51**, 8999–9006.
41 P. A. Quinto-Su, M. Suzuki and C.-D. Ohl, *Scientific reports*, 2014, **4**, 5445.
42 C.-H. Tai, R.-J. Yang, M.-Z. Huang, C.-W. Liu, C.-H. Tsai and L.-M. Fu, *Electrophoresis*, 2006, **27**, 4982–4990.
43 A. D. Stroock, S. K. W. Dertinger, A. Ajdari, I. Mezic, H. A. Stone and G. M. Whitesides, *Science (New York, N.Y.)*, 2002, **295**, 647–651.
44 R. D. Keane and R. J. Adrian, *Applied Scientific Research*, 1992, **49**, 191–215.
45 H. Kinoshita, S. Kaneda, T. Fujii and M. Oshima, *Lab on a chip*, 2007, **7**, 338–346.
46 Nickolaj J. Petersen, Klaus B. Mogensen, Jörg P. Kutter, *Electrophoresis*, 2001, **23**, 3528–3536.
47 J. Yue, F. H. Falke, J. C. Schouten and T. A. Nijhuis, *Lab on a chip*, 2013, **13**, 4855–4863.
48 J. Wagner, T.R. Tshikhudo, J.M. Köhler, *Chemical Engineering Journal*, 2008, **135**, S104-S109.
49 G. Peybernès, R. Grossier, F. Villard, P. Letellier, M. Lagaize, N. Candoni and S. Veesler, *Org. Process Res. Dev.*, 2018, **22**, 1856–1860.
50 T. Pan, R. T. Kelly, M. C. Asplund and A. T. Woolley, *Journal of Chromatography A*, 2004, **1027**, 231–235.
51 M. V. Barich and A. T. Krummel, *Analytical chemistry*, 2013, **85**, 10000–10003.
52 C. Wagner, W. Buchegger, M. Vellekoop, M. Kraft and B. Lendl, *Anal Bioanal Chem*, 2011, **400**, 2487–2497.
53 D. P. Kise, D. Magana, M. J. Reddish and R. B. Dyer, *Lab Chip*, 2014, **14**, 584–591.
54 K. L. A. Chan and S. G. Kazarian, *The Analyst*, 2013, **138**, 4040–4047.
55 P. Svasek, E. Svasek, B. Lendl and M. Vellekoop, *Sensors and Actuators A: Physical*, 2004, **115**, 591–599.
56 C.-K. Chen, M.-H. Chang, H.-T. Wu, Y.-C. Lee and T.-J. Yen, *Biosensors & bioelectronics*, 2014, **60**, 343–350.
57 K. L. A. Chan, X. Niu, A. J. de Mello and S. G. Kazarian, *Lab Chip*, 2010, **10**, 2170.
58 E. Polshin, B. Verbruggen, D. Witters, B. Sels, D. de Vos, B. Nicolaï and J. Lammertyn, *Sensors and Actuators B: Chemical*, 2014, **196**, 175–182.
59 K. L. A. Chan, X. Niu, A. J. deMello and S. G. Kazarian, *Analytical chemistry*, 2011, **83**, 3606–3609.
60 Z. Wang, D. Voicu, L. Tang, W. Li and E. Kumacheva, *Lab on a chip*, 2015, **15**, 2110–2116.
61 A. V. Ewing, G. S. Clarke and S. G. Kazarian, *Biomicrofluidics*, 2016, **10**, 24125.
62 A. Perro, G. Lebourdon, S. Henry, S. Lecomte, L. Servant and S. Marre, *React. Chem. Eng.*, 2016, **1**, 577–594.
63 T. Ohsaka, S. Yamaoka, O. Shimomura, *solid state communication*, 1979, **30**, 345–347.
64 Y. Lin, X. Yu, Z. Wang, S.-T. Tu and Z. Wang, *Analytica chimica acta*, 2010, **667**, 103–112.
65 N. Liu, C. Aymonier, C. Lecoutre, Y. Garrabos and S. Marre, *Chemical Physics Letters*, 2012, **551**, 139–143.

66 S. K. Luther, S. Stehle, K. Weihs, S. Will and A. Braeuer, *Analytical chemistry*, 2015, **87**, 8165–8172.
67 Y. Jun Kang, E. Yeom and S.-J. Lee, *Biomicrofluidics*, 2013, **7**, 54111.
68 Y. J. Kang, S. Y. Yoon, K.-H. Lee and S. Yang, *Artificial organs*, 2010, **34**, 944–949.
69 Y. Jun Kang, J. Ryu and S.-J. Lee, *Biomicrofluidics*, 2013, **7**, 44106.
70 W. J. Lan, S. W. Li, J. H. Xu and G. S. Luo, *Microfluid Nanofluid*, 2010, **8**, 687–693.
71 S. Kim, K. C. Kim and E. Yeom, *Optics and Lasers in Engineering*, 2018, **104**, 237–243.
72 Formulaction Inc., *Visual flow rheology by microfluidics,* available at: http://www.formulaction.com/files/instruments/brochures/doc_a4_fluidicam.pdf.
73 N. Srivastava, R. D. Davenport and M. A. Burns, *Analytical chemistry*, 2005, **77**, 383–392.
74 N. Srivastava and M. A. Burns, *Analytical chemistry*, 2006, **78**, 1690–1696.
75 O. Cakmak, C. Elbuken, E. Ermek, A. Mostafazadeh, I. Baris, B. Erdem Alaca, I. H. Kavakli and H. Urey, *Methods (San Diego, Calif.)*, 2013, **63**, 225–232.
76 G. Dehestru, M. Leman, J. Jundt, P. Dryden, M. Sullivan and C. Harrison, *The Review of scientific instruments*, 2011, **82**, 35113.
77 N. Srivastava and M. A. Burns, *Lab on a chip*, 2006, **6**, 744–751.
78 Z. Wang, L. Tan, X. Pan, G. Liu, Y. He, W. Jin, M. Li, Y. Hu and H. Gu, *ACS applied materials & interfaces*, 2017, **9**, 28586–28595.
79 B. Pinho, S. Girardon, F. Bazer-Bachi, G. Bergeot, S. Marre and C. Aymonier, *The Journal of Supercritical Fluids*, 2015, **105**, 186–192.
80 O. Cakmak, E. Ermek, N. Kilinc, G. G. Yaralioglu and H. Urey, *Sensors and Actuators A: Physical*, 2015, **232**, 141–147.
81 M. F. Khan, S. Schmid, P. E. Larsen, Z. J. Davis, W. Yan, E. H. Stenby and A. Boisen, *Sensors and Actuators B: Chemical*, 2013, **185**, 456–461.
82 A. E. Kamholz and P. Yager, *Biophysical Journal*, 2001, **80**, 155–160.
83 F. Hossein-Babaei, A. Hooshyar Zare and V. Ghafarinia, *Sensors and Actuators B: Chemical*, 2016, **233**, 646–653.
84 T. Hotta, S. Nii, T. Yajima and F. Kawaizumi, *Chem. Eng. Technol.*, 2007, **30**, 208–213.
85 J. Jiménez, *J. Fluid Mech.*, 2005, **535**, 245–254.
86 J.-B. Salmon, A. Ajdari, P. Tabeling, L. Servant, D. Talaga and M. Joanicot, *Appl. Phys. Lett.*, 2005, **86**, 94106.
87 E. Häusler, P. Domagalski, M. Ottens and A. Bardow, *Chemical Engineering Science*, 2012, **72**, 45–50.
88 G. Franceschini and S. Macchietto, *Chemical Engineering Science*, 2008, **63**, 4846–4872.
89 L. Wolff, H.-J. Koß and A. Bardow, *Chemical Engineering Science*, 2016, **152**, 392–402.
90 M. Dou, J. M. García, S. Zhan and X. Li, *Chemical communications (Cambridge, England)*, 2016, **52**, 3470–3473.
91 B. T. C. Lau, C. A. Baitz, X. P. Dong and C. L. Hansen, *Journal of the American Chemical Society*, 2007, **129**, 454–455.
92 S. Morais, N. Liu, A. Diouf, D. Bernard, C. Lecoutre, Y. Garrabos and S. Marre, *Lab on a chip*, 2016, **16**, 3493–3502.
93 B. Bao, J. Riordon, F. Mostowfi and D. Sinton, *Lab on a chip*, 2017, **17**, 2740–2759.
94 M. Abolhasani, M. Singh, E. Kumacheva and A. Gunther, *Lab on a chip*, 2012, **12**, 1611–1618.
95 S. G. R. Lefortier, P. J. Hamersma, A. Bardow and M. T. Kreutzer, *Lab on a chip*, 2012, **12**, 3387–3391.
96 M. Sauzade and T. Cubaud, *Physical review. E, Statistical, nonlinear, and soft matter physics*, 2013, **88**, 51001.
97 A. Sell, H. Fadaei, M. Kim and D. Sinton, *Environmental science & technology*, 2013, **47**, 71–78.
98 H. Fadaei, J. M. Shaw and D. Sinton, *Energy Fuels*, 2013, **27**, 2042–2048.
99 V. J. Sieben, A. K. Tharanivasan, S. I. Andersen and F. Mostowfi, *Energy Fuels*, 2015, **30**, 1933–1946.
100 B. Pinho and R. L. Hartman, *React. Chem. Eng.*, 2017, **2**, 189–200.
101 C. Xu and T. Xie, *Ind. Eng. Chem. Res.*, 2017, **56**, 7593–7622.
102 J. G. Kralj, H. R. Sahoo and K. F. Jensen, *Lab on a chip*, 2007, **7**, 256–263.
103 A. Sahu, A. B. Vir, L. S. Molleti, S. Ramji and S. Pushpavanam, *Chemical Engineering and Processing: Process Intensification*, 2016, **104**, 190–200.
104 N. Assmann, S. Kaiser and P. Rudolf von Rohr, *The Journal of Supercritical Fluids*, 2012, **67**, 149–154.
105 S. Ogden, R. Bodén, M. Do-Quang, Z. G. Wu, G. Amberg and K. Hjort, *Microfluid Nanofluid*, 2014, **17**, 1105–1112.
106 S. K. Luther and A. Braeuer, *The Journal of Supercritical Fluids*, 2012, **65**, 78–86.
107 J. B. Kuenen, *Phil. Mag.*, 1897, **44, 174**.
108 Fred H Poettmann, D. L. Katz, *University of Michigan, Ann Arbor, Mich.*, 1945.
109 W. B. Kay, 1968.
110 Jack J. C. Hsu, N. Nagarajan and and R. L. Robinson Jr., *J. Chem. Eng. Data*, 1986, **32 (2)**, 168–172.
111 S. Molla and F. Mostowfi, in *SPE Annual Technical Conference and Exhibition*, 2014.
112 M. T. Sullivan and D. E. Angelescu, *Energy Fuels*, 2016, **30**, 2655–2661.
113 S. Gruener and P. Huber, *Physical review letters*, 2009, **103**, 174501.
114 J. Ally, S. Molla and F. Mostowfi, *Langmuir : the ACS journal of surfaces and colloids*, 2016, **32**, 4494–4499.